8-band k.p modeling of the quantum confined Stark effect in Ge quantum wells on Si substrates

D.J. Paul*
University of Glasgow, Department of Electronics and Electrical Engineering, Oakfield Avenue, Glasgow, G12 8LT, U.K.
(Dated: February 13, 2008)

Recent work using compressively strained-Ge quantum wells grown on $Si_{1-y}Ge_y$ virtual substrates has demonstrated efficient modulation on a silicon substrate through the quantum confined Stark effect with performance comparable to many direct bandgap III-V materials. The absorption of compressively strained-Ge quantum wells is calculated using an 8-band **k.p** solver within the envelope function technique. The calculated absorption spectra provide excellent agreement with experimental results, demonstrating that the absorption is dominated by the direct bandgap and allow a number of predictions of the absorption for different polarizations, quantum well widths, electric fields and strain to be calculated. It is also shown that some of the experimental results in the literature require tensile strained substrates to produce agreement with the theoretical calculations.

PACS numbers: 71.35.Cc, 73.21.Fg, 78.20.Bh

I. INTRODUCTION

While silicon dominates the electronics market, the lack of an efficient light emitter or modulation effect has prevented complete silicon optoelectronic solutions from being realised. The indirect bandgap of silicon results in significantly smaller electro-optical effects[1, 2] than those in direct bandgap III-V materials. Silicon photonics as a field has grown enormously in the last decade especially as copper interconnects on and off silicon chips are close to reaching the theoretical maximum bandwidths and new optical solutions are required for low cost, higher bandwidth performance from microelectronic systems[2]. Modulators have been demonstrated on silicon using the Franz-Keldysh effect[2] and the stronger free carrier plasma effect[1–4] but all demonstrated devices still have poorer performance or larger sizes than equivalent III-V devices at the important 1.55 μm operating wavelength.

Recently the quantum confined Stark effect (QCSE) was demonstrated using strained-Ge quantum wells grown on top of a silicon wafer[5, 6]. The QCSE can be considered as the analog of the Franz-Keldysh effect for electrons and holes confined in a type I quantum well so that bound excitonic effects strongly effect the absorption properties of the device[7, 8]. The work on strained-Ge quantum wells[9] suggests that the direct electron Γ-valley transitions to hole states dominate the optical absorption properties of these systems as the zone-centre Γ_{7c}^{-}-valley for electrons is only about 140 meV above the L-valley conduction band edge.

In this paper, the absorption of compressively strained-Ge quantum wells is calculated using an 8-band **k.p**-solver[10]. The results demonstrate that the absorption is indeed dominated by the direct bandgap and the modeling tool is used to calculate the absorption edge for a number of different quantum well widths and strain conditions. The polarization dependence of the absorption is also calculated demonstrating the difference between surface-normal (xy-polarization) and ridge waveguide (z-polarization) devices. One major issue which will be demonstrated is that a number of the published results require a strained virtual substrate rather than an unstrained virtual substrate to agree with the theory.

II. DESCRIPTION OF MODELING TECHNIQUE

The absorption was calculated using the band structure tool Nextnano[10] using an 8-band **k.p** solver. The technique is similar to the envelope function technique derived by Bastard[11] and a full derivation of the absorption coefficient, $\alpha(\omega)$ as a function of angular frequency, ω can be found in Ref. [10]. The basis states are S-like for the Γ_{7c}^{-}-conduction band and P-like for the valence band with each state with spin degeneracy of 2 giving the eight bands of $|S\uparrow\rangle$, $|X\uparrow\rangle$, $|Y\uparrow\rangle$, $|Z\uparrow\rangle$, $|S\downarrow\rangle$, $|X\downarrow\rangle$, $|Y\downarrow\rangle$, $|Z\downarrow\rangle$. The absorption result is from the projection of the susceptibility tensor, χ_{ij} onto the polarization vector, ε_j of the incident light to produce

$$\alpha(\omega) = \frac{4\pi\omega}{nc}\varepsilon_i^* \chi_{ij}(\omega)\,\varepsilon_j \tag{1}$$

where n is the refractive index and c the speed of light. The susceptibility (only the imaginary part is required for absorption and is quoted after symmetry and selection rules have been used to reduce the form) is given by

$$\chi_{ij}(\omega) = \frac{i\pi e^2\hbar^2}{m^2\omega^2\Omega}\frac{1}{4\pi\varepsilon_0}\frac{E_p m_0}{2\hbar^2}\frac{S}{a_0^2}\left(\frac{a_0 k_{max}}{\pi}\right)^2 \times \sum_{n,n',\sigma}\int d\mathbf{k}_\perp |\langle n,k,\sigma,i|n',k,\sigma,i\rangle^*\langle n,k,\sigma,j|n',k,\sigma,j\rangle|^2 \tag{2}$$

*Electronic address: D.Paul@elec.gla.ac.uk

TABLE I: The input parameters used in the 8-band **k.p** modeling.

Parameter	Silicon	Germanium
Lattice constant, a (nm)	0.54304[a]	0.56579[a]
Elastic constant, c_{11} (GPa)	165.77[a]	128.53[a]
Elastic constant, c_{12} (GPa)	63.93[a]	48.28[a]
Elastic constant, c_{44} (GPa)	79.62[a]	66.80[a]
Varshni α_Γ (meV/K)	0.5367[b]	0.6842[b]
Varshni β_Γ (K)	745.8[b]	398[b]
Varshni α_L (meV/K)	0.5367[b]	0.4561[b]
Varshni β_L (K)	745.8[b]	210[b]
Kane matrix element, E_p (eV)	26.92[a]	25.49[a]
Kane parameter, S (eV)	1	1
a_v (eV)	1.80[c]	1.24[c]
b (eV)	-2.10[d]	-2.86[e]
d (eV)	-4.85[d]	-5.28[e]
a_c^Γ (eV)	-10.39[f]	-10.41[f]
a_c^L (eV)	-0.66[g]	-1.54[g]
a_c^X (eV)	3.3[h]	2.55[g]
Ξ_u^Γ	0.0	0.0
Ξ_u^L	16.14[g]	16.2[i]
Ξ_u^Δ	8.6[d]	9.42[g]
L' ($\frac{\hbar^2}{2m_0^*}$)	-6.69[j]	-31.34[j]
M' ($\frac{\hbar^2}{2m_0^*}$)	-4.62[j]	-5.90[j]
N' ($\frac{\hbar^2}{2m_0^*}$)	-8.56[j]	-34.14[j]
Δ (meV)	44[a]	289[a]

[a]Reference [12]
[b]Reference [13]
[c]Reference [14]
[d]Reference [15]
[e]Reference [16]
[f]Reference [17]
[g]Reference [18]
[h]Reference [19]
[i]Reference [20]
[j]Reference [21]

for a transition from state n to n' at wavenumber k with spin σ and polarization i or j. The variables above are as follows: e is the electronic charge, $\hbar$ is Planck's constant divided by 2π, m is the effective mass, m_0 is the free electron mass, E_p is the Kane matrix element defined in terms of the momentum Hamiltonian as $\frac{2}{m_0}|\langle S\downarrow|\hat{p}_x|X\downarrow\rangle|^2$, S is the Kane parameter, a_0 is the Bohr radius, k_{max} is the maximum $k_{||}$ wavenumber, ε_0 is the permittivity of free space and Ω is the volume of the sample.

The major input parameters for the calculations are listed in table I. Where possible experimentally derived or measured input parameters have been used[22] although these were not available for a number of parameters. Unlike direct bandgap III-V materials which have a large literature of parameters for 8-band **k.p** tools[23], the indirect materials of Si and Ge make the extraction of some of these parameters difficult[22]. For this work the standard 6-band Dresselhaus parameters from Ref. 21 were used and they were not scaled to the 8-band values as described in Ref. [10] for III-V materials. The inversion symmetry operator was set to zero, the Kane parameter, S was set to 1 eV and the values of the Kane matrix element, E_p were derived at 4.2 K for Si and 10 K for Ge using experimental data from Ref. 12. All values were linearly extrapolated between Si and Ge values for $Si_{1-x}Ge_x$ layers except the Dresselhaus parameters which were bowed using the scheme in Ref. 21 since these values provide excellent agreement between the simulations and experimental intersubband hole absorption and emission results in refs. 12, 24–27. The coupling between the conduction and valence band is therefore dominated by the Kane matrix element, E_p in the present work. While some of these parameters are not used in the standard III-V way for 8-band **k.p** simulations[23], the agreement between experiment and theory which will be demonstrated later provides the justification for the selection and present use of the parameters.

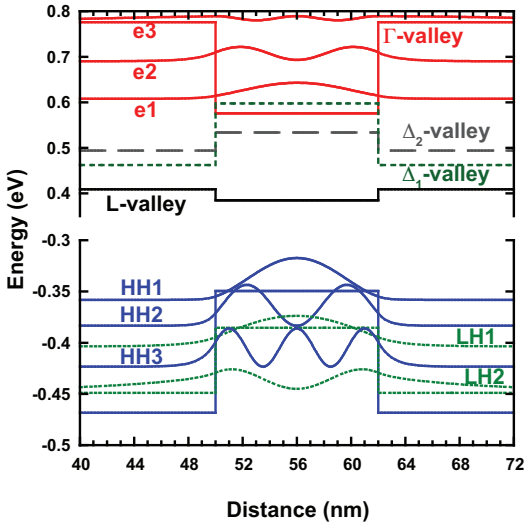

FIG. 1: The band structure for the compressively strained-12 nm quantum well[9] showing the band edges and squared wavefunctions for the lowest energy subband states for the Γ_{7c}^-, HH and LH subbands.

III. DEVICES WITHOUT ELECTRIC FIELDS

The first structure to be modeled was a 12 nm compressively strained Ge quantum well sandwiched between 24 nm thick tensile strained-$Si_{0.15}Ge_{0.85}$ barriers and grown on top of a linearly-graded, relaxed $Si_{0.1}Ge_{0.9}$ virtual substrate[9]. For this particular structure, the experimental results in Ref. 9 are for flat band conditions without an applied electric field at 17 K. Fig. 1 shows the calculated band edges and lowest energy subband states for the heavy-hole (HH), light-hole (LH) and Γ_{7c}^- conduction band electrons. Also shown are the band edges for the L- and Δ-valleys. The split-off (SO) band is too low in energy to be plotted and does not play any significant role in the absorption process although as with all strained-SiGe structures, there is significant mixing

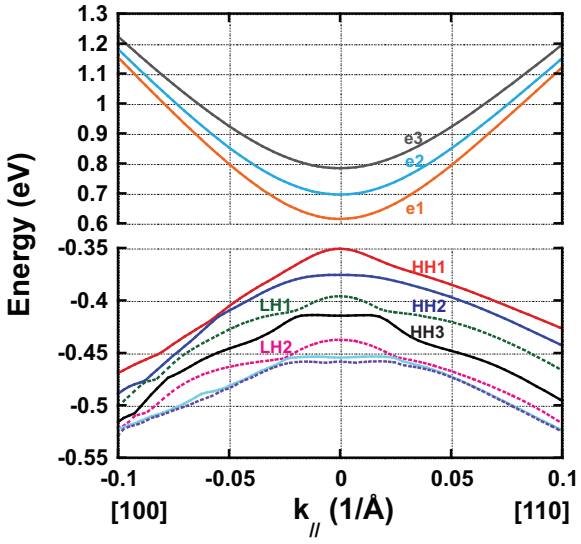

FIG. 2: The in-plane subband dispersion of the electron and holes states along the [100] and [110] directions.

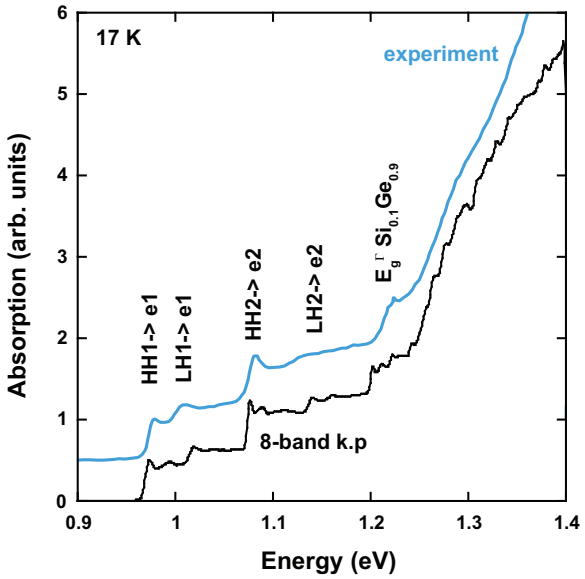

FIG. 3: The xy-polarised spectra for the PSI 12 nm Ge quantum well grown on $Si_{0.1}Ge_{0.9}$ virtual substrate with $Si_{0.15}Ge_{0.85}$ barriers and 0 V/m electric field at 17 K. The curves are offset for clarity.

between the SO and LH states due to the off diagonal terms in the 8-band Hamiltonian. While strictly speaking these should be described as LH/SO subbands, for brevity they will be described as LH states from now on.

Fig. 2 shows the in-plane dispersion of both the electron and hole subband states for those closest to the band edge transitions. While the electron dispersions are close to parabolic, the hole states are clearly non-parabolic. The selection rules assuming parabolic dispersions of the subbands with the xy-polarisation (TE) of the present experimental results allow the following transitions[11]: HH1-e1, HH2-e2, LH1-e1, LH2-e2, etc.... While non-parabolicity can allow weak transitions at finite $k_{\|}$ from forbidden transitions in the parabolic approximation, none of the calculated absorption spectra in this work show any significant absorption from relaxation of those forbidden transitions for the main excitonic features.

The absorption spectra were calculated up to a maximum k-parallel value of 1.1 nm^{-1} with 961 k-parallel points for Brillouin zone discretization. Spectra were calculated for 1,2 and 5 quantum wells with little difference being found in the calculated absorption spectra for different numbers of quantum wells. Hence all subsequent absorption spectra will be calculated using a single quantum well which has the minimum computational resource requirements. Fig. 3 shows the absorption spectra at 17 K for a single quantum well and spacers of 20 nm on each side of the quantum well assuming 1 meV of broadening compared to the experimental results in Ref. 9. The main transitions are also annotated on the figure and excellent agreement is shown between the calculated and experimental spectra for many of these transitions.

The experimental data in Fig. 3 was compared to absorption spectra calculated by 6-band **k.p** for the hole states and a single-electron effective mass calculation for the electrons in the original paper[9]. While this calculation produced excellent agreement for the lowest absorption peak observed experimentally at 0.978 eV, many of the other transitions were at significantly different energies to the experimental results. The present 8-band solutions using literature input values and no fitting parameters produces the first absorption peak at 0.973 eV and has better agreement with the higher transitions as would be expected with the addition of coupling between the electron and hole states. The present calculations also reproduce the absorption peak around 1.25 eV by extending the eigenvalue calculation to a 20 nm layer adjacent to the spacer and quantum well system with the composition of the relaxed $Si_{0.1}Ge_{0.9}$ virtual substrate. This peak was missing in the 6-band calculation[9] which only calculated the absorption for the Ge quantum well.

At present the model uses a linear interpolation between Si and Ge for the bandgap energy which produces the $Si_{0.1}Ge_{0.9}$ virtual substrate absorption peak close to 1.20 eV compared to the experimental 1.25 eV suggesting that bowing of the bandgap energy is required for more accurate modeling of the substrate peak. The electron to HH absorption peaks are more accurately calculated by the model than the transitions to LH states. The HH subband state energies are related to first order to the well widths while the energies of the LH states are much more related to the Ge content and are more strain dependent. The poorer fit to the electron to LH transitions also suggests that accurate bowing parameters are required for the bandgap, deformation and Dresselhaus parameters to provide more accurate predictions. At present there is little $Si_{1-x}Ge_x$ data in the literature at these high Ge contents to allow accurate parameters to be experimen-

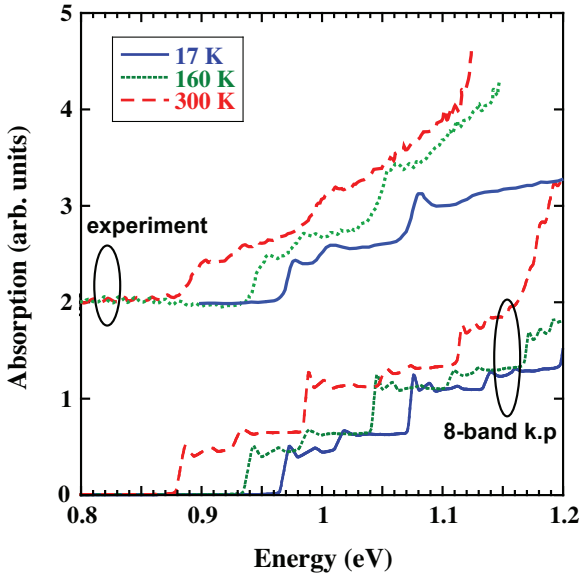

FIG. 4: The temperature dependence of the xy-polarised spectrum as a function of temperature for the PSI 12 nm Ge quantum well grown on $Si_{0.1}Ge_{0.9}$ virtual substrate with $Si_{0.15}Ge_{0.85}$ barriers and 0 V/m electric field.

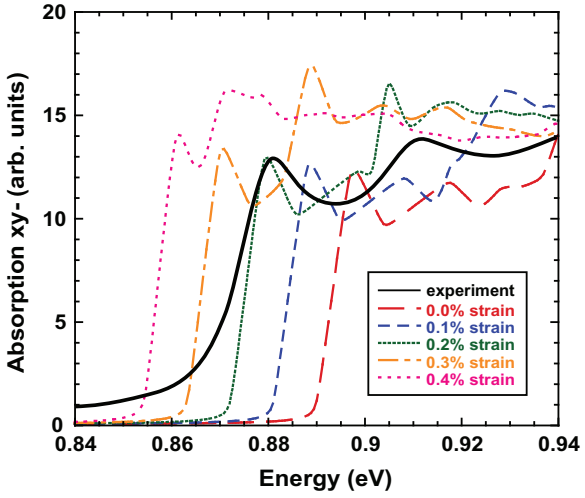

FIG. 5: The xy-polarised absorption spectrum at 300 K for a 10 nm Ge quantum well on a $Si_{0.1}Ge_{0.9}$ virtual substrate with $Si_{0.15}Ge_{0.85}$ barriers with an electric field of 1.63 MV/m at 300 K. The solid black line is experimental data plotted from Ref. 5 while the dashed colored lines are for the 8-band **k.p** solutions with different levels of tensile strained substrate.

tally determined.

The modeled absorption curve in Fig. 3 also shows very weak transitions at some of the forbidden transitions which are not observed in the experimental results. Firstly the modeled curve could have a larger smoothing factor added which would more closely resemble the experimental results but also the non-parabolicity which is required to break the selection rules may be different in the real sample compared to the model due to the bowing of the parameters discussed in the previous paragraph. Also above about 1.25 eV, the modeled curve shows discrete transitions due to the finite number of states calculated which could be smoothed out by greatly increasing the number of quantum state solutions for the continuum but at the expense of greatly increased computational time.

The temperature dependence of the absorption spectra was also calculated using the model of Varshni[13] to account for the change in bandgap where

$$E_g(T) = E_g(T=0) - \frac{\alpha T^2}{T+\beta} \qquad (3)$$

The data used for the bandgaps at different symmetry points and the fitting parameters, α and β are listed in table I and the resulting absorption spectra calculated using the data are compared to experiment in Fig. 4. The agreement for the absorption edge from 17 K to 300 K is excellent even though no additional broadening over the 1 meV value has been added to the higher temperature calculations. It is clear that some form of additional broadening is required, especially for the higher energy transitions, if better fitting is required to the experimental data. The present results suggest that the broadening increases with temperature but there are also, as will be discussed later, indirect absorption effects which also increase with increasing temperature.

IV. DEVICES WITH ELECTRIC FIELDS

The original paper on the Ge well QCSE used 10 quantum wells inside a p-i-n structure which results in a built in electric field of 1.63 MV/m with 0 V applied across the p-i-n device[5]. The distance between p- and n-contact regions was 460 nm. To model this structure a single quantum well was used with a constant electric field applied across the structure before the eigenstates were calculated. The calculated absorption spectrum is compared to the experimental data in Fig. 5. It was clear from the initial calculation of compressive-Ge quantum well and tensile spacers being commensurate to a relaxed $Si_{0.1}Ge_{0.9}$ substrate (0% strain in Fig. 5) did not match the experimental data. Unlike the first sample from Ref. 9 which was grown on a ∼13 μm thick linearly graded strain relaxation buffer where the grading rate was 7% Ge/μm, the experimental data in Fig. 5 came from a sample with a thin virtual substrate of only 500 nm thickness[22]. This thin buffer was grown at low temperature and then annealed at high temperature to relax. A number of papers[28, 29] have demonstrated that such fabrication results in tensile strain and not complete relaxation in the buffer and therefore the lattice constant is not that of bulk, relaxed $Si_{0.1}Ge_{0.9}$. Up to 0.2% tensile strain has been demonstrated just by annealing Ge heterolayers while the addition of further processing steps

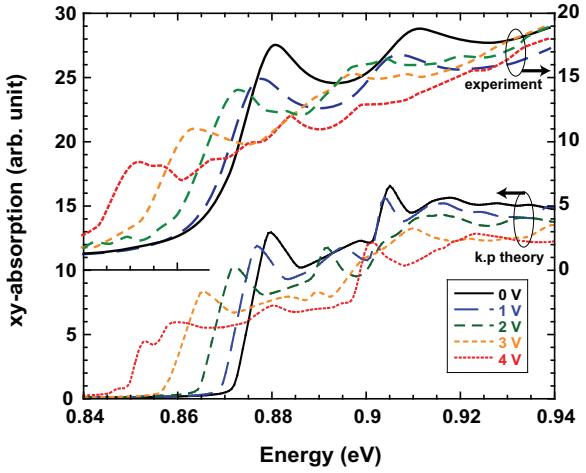

FIG. 6: The xy-polarised absorption spectrum at 300 K for a 10 nm Ge quantum well on a $Si_{0.1}Ge_{0.9}$ virtual substrate with $Si_{0.15}Ge_{0.85}$ barriers as a function of electric field at 300 K. Curves at the bottom of the figure are as calculated by 8-band **k.p** theory assuming a 0.2% tensile strained substrate and curves at the top of the figure are experimental data from Ref. 5. The theory and experimental curves are offset for clarity.

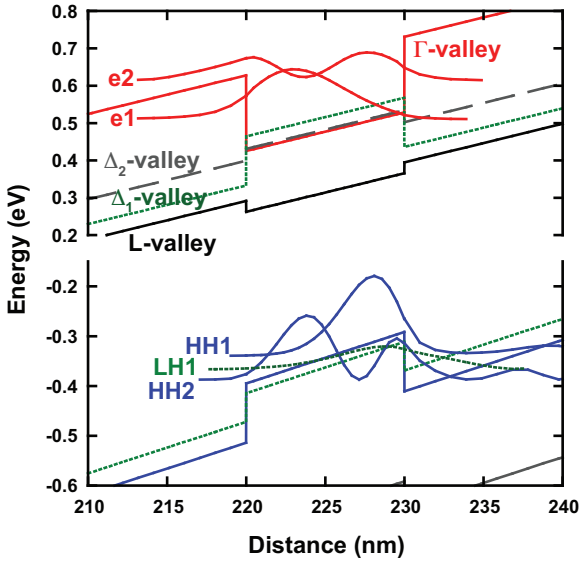

FIG. 7: The band structure for 4 V applied (10.3 MV/m) to a 10 nm Ge quantum well with the Stark shift clearly evident for the squared wavefunctions of the lowest energy electron and hole states. The wavefunctions have been scaled to 2.5 times the height in Fig. 1 to aid clarity.

such as backside silicidation has shown tensile strain up to 0.25%[28].

To account for this tensile strain, the absorption spectra were calculated for different levels of tensile strain in the virtual substrate. This was achieved by calculating the appropriate lattice constant for each level of tensile strain in a $Si_{0.1}Ge_{0.9}$ layer and then fixing the substrate lattice constant to this value before commensurately straining the quantum wells, barriers and spacers on top. The results for tensile strain levels in the substrate from 0 to 0.4% are plotted against the experimental results in Fig. 5 and the best fit for the main HH1-e1 absorption peak was obtained using 0.2% tensile strain. This is very similar to the values reported for similar strain relaxation buffers made out of pure Ge in Ref. 28 rather than $Si_{0.1}Ge_{0.9}$. For operation of modulators at the important 1.55 μm band (0.807 eV), tensile strain is beneficial in moving the absorption edge to lower energy or longer wavelength. It is also clear from Fig. 5 that the experimental results have a significantly larger tail below the HH1-e1 absorption peak than the modeled results. Expanding the broadening of the peak did not allow accurate modeling of this tail and it is believed to be related to indirect absorption between the L-valley and hole states.

Fig. 6 compares the experimental and modeled results for absorption as a function of applied bias for the 10 nm Ge quantum well modulator in Ref. 5. The calculated absorption shows good agreement with the experiment although that agreement becomes poorer as the voltage and therefore electric field is increased. This is not surprising as the larger electric fields will result in more heating in the sample and this would result in a

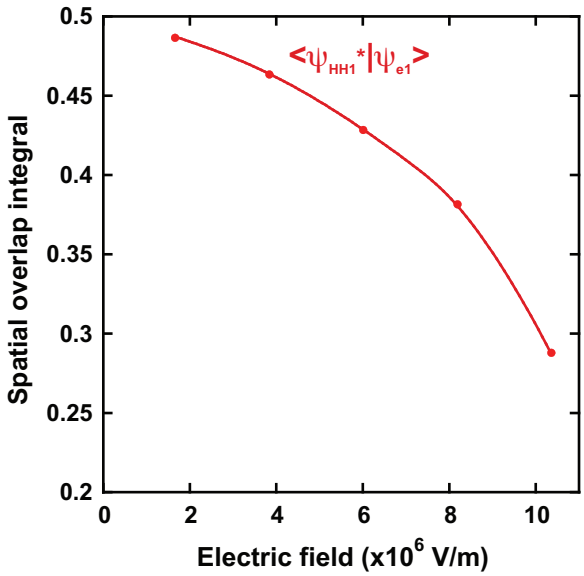

FIG. 8: The spatial overlap integral between the lowest electron and lowest HH states as a function of electric field for a 10 nm Ge quantum well at 300 K. The values quoted are the mean for both spin states for each spin degenerate subband.

higher probability of indirect absorption with the larger number of phonons in the system. As the indirect transition is about 140 meV lower in energy than the direct transition, this will produce a tail below the direct HH1-e1 transition. To model this tail accurately will require another technique as the 8-band **k.p** technique is limited to direct transitions in the system.

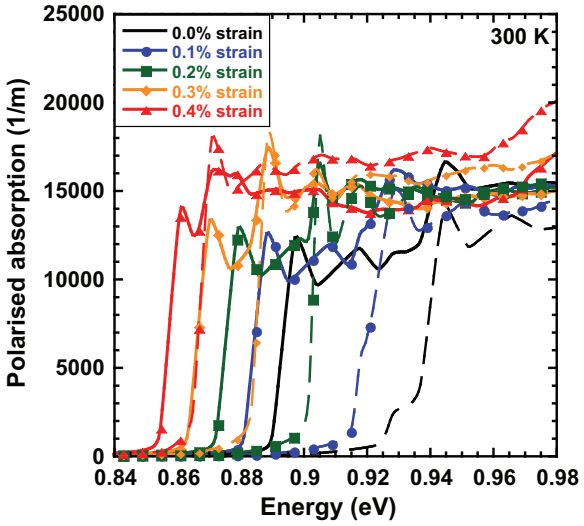

FIG. 9: The calculated absorption spectrum at 300 K for a 10 nm Ge quantum well on a $Si_{0.1}Ge_{0.9}$ virtual substrate with $Si_{0.15}Ge_{0.85}$ barriers, an electric field of 1.63 MV/m at 300 K and different levels of tensile strained substrate. Solid lines are xy-polarization and dashed lines are z-polarization.

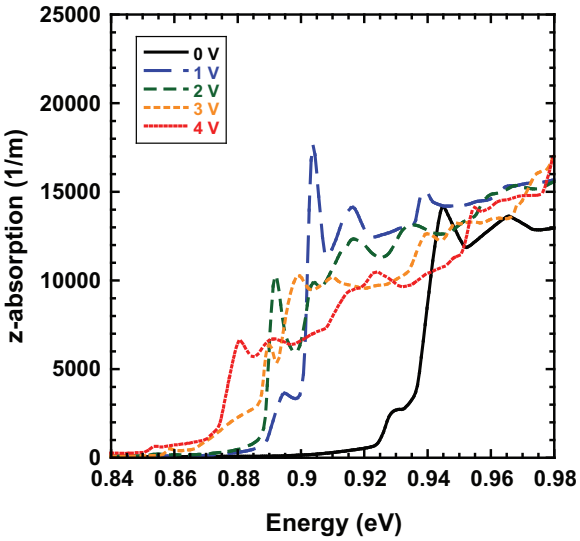

FIG. 10: The z-polarised absorption spectrum at 300 K for a 10 nm Ge quantum well on a $Si_{0.1}Ge_{0.9}$ virtual substrate with $Si_{0.15}Ge_{0.85}$ barriers with voltage applied across a 460 nm p-i-n device region at 300 K. A 0.2% tensile strained substrate was assumed.

The application of a Stark shift is expected to reduce the overlap of the electron and hole wavefunctions as the electric field is increased (see Fig. 7). To try to get a quantitative idea of the change in this overlap, the spatial overlap integral, $\langle \psi^*_{HH1} | \psi_{e1} \rangle$ was calculated for the 4 experimental applied voltages from 0 V to 4 V. To reduce boundary effects, the **k.p** solution to Schrödinger's equation was expanded to a distance 50 nm each side of the quantum well. The results for the lowest subband states are plotted in Fig. 8 as a function of electric field. It is clear that the spatial overlap between the lowest electron and HH subbands reduces by a factor of 0.59 between 0 and 4 V applied across the p-i-n device. It should also be noted in Fig. 7 that the mixed LH/SO states are much more weakly confined than the HH states due to the lower heterostructure discontinuity. More detailed analysis of the modeled results suggest that by 4 V, only the lowest electron subband does not have any significant coupling to continuum states.

V. POLARIZATIONS DEPENDENCE OF ABSORPTION

All the experimental results published for Ge quantum well modulators have used the surface-normal xy-polarisation as this is the easiest to measure. There are many systems where waveguide geometry devices with z-polarisation (TM) are useful. Fig. 9 shows the absorption spectra for both xy- and z-polarisations for five different levels of tensile strained substrates calculated with the present 8-band **k.p** tool. The selection rules are of course different for the z-polarization with the lowest dominant transition peak at flat bands being the LH/SO1-e1 transition with the HH1-e1 transition forbidden in the parabolic approximation[11]. The difference in selection rules results in the z-polarized absorption being at higher energy although as the tensile strain in the substrate is increased, the difference between the xy- and z-polarization is reduced as the LH/SO1 state becomes closer in energy to the HH1 state. If sufficient tensile strain could be applied (above approximately 0.6%) then for the present device, the z-polarization would end up with a lower energy absorption edge when the LH/SO1 state is higher in electron energy (lower in hole energy) than the HH1 state. It is, however, not clear at present how such high levels of tensile strain could be achieved in a practical experimental device in the SiGe system.

Fig. 10 shows the calculated z-polarised absorption spectrum for the 10 nm Ge quantum well device as a function of applied electric field in Ref. 6. The operation of the device is at higher energy (lower wavelength) than the xy-polarization device but the shift in the excitonic absorption peak is much larger at lower electric fields. It is clear that for longer wavelength (lower energy) operation of a modulator different levels of Ge content, strain and / or quantum well width are required if 1.55 μm operation is to be achieved.

VI. PREDICTIONS FOR GERMANIUM CONTENT AND QUANTUM WELL THICKNESS

In the final section of this paper, the 8-band **k.p** tool will be used to map out parts of the appropriate parameter space for making Ge-quantum well QCSE modulators. The most important wavelength for photonics is

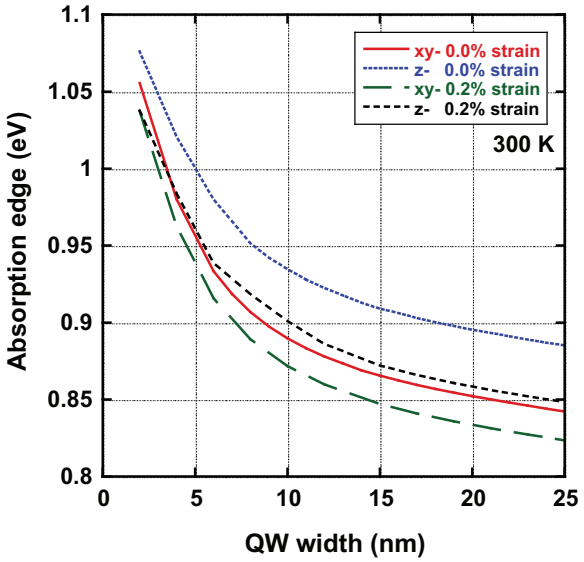

FIG. 11: The absorption edge as a function of Ge quantum well width on $Si_{0.1}Ge_{0.9}$ virtual substrates with $Si_{0.15}Ge_{0.85}$ barriers with an electric field of 1.63 MV/m at 300 K.

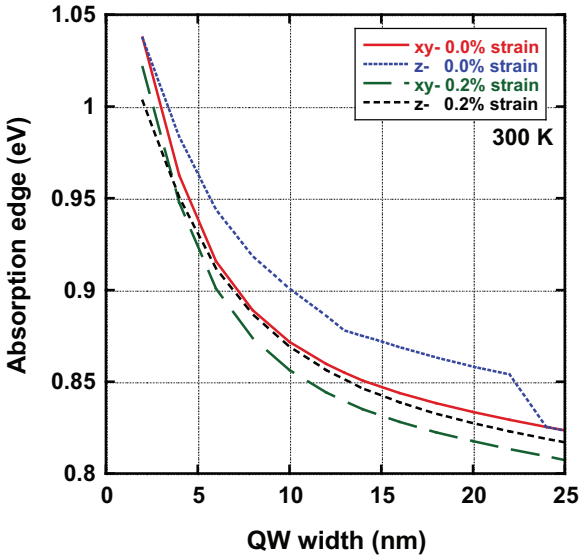

FIG. 12: The absorption edge as a function of Ge quantum well width on $Si_{0.05}Ge_{0.95}$ virtual substrates with an electric field of 1.63 MV/m at 300 K.

1.55 μm which corresponds to 0.807 eV in energy. An ideal modulator would have the main absorption peak slightly higher in energy than 0.807 eV and be swept through this value to a lower energy with the application of a small applied bias. It is clear from the above results and as shown in Refs. 6, 7 that a lower Ge content virtual substrate and wider quantum well are required for longer wavelength operation. Therefore the absorption was calculated for different quantum well thicknesses for tensile strained and relaxed substrates of both $Si_{0.1}Ge_{0.9}$ and $Si_{0.05}Ge_{0.95}$ compositions. The results are plotted in Figs. 11 and 12.

To be consistent for both xy- and z-polarized calculations especially when strain in the substrate can result in anti-crossing of subband states, non-parabolicity and mixing leading to multiple peaks near the absorption edge, the absorption edge has been defined as where the linear extrapolational of the lowest, distinct, direct-transition energy absorption peak edge crosses the energy axis. This may not be the best definition but does provide consistency to plot values on a single graph when band mixing of both HH and LH/SO states can relax selection rules resulting in small absorption compared to the main exciton peak as can be observed in Fig. 10 for 1 V applied bias. The modeling results suggests that using a 0.2% tensile strained substrate of $Si_{0.05}Ge_{0.95}$ composition combined with a Ge quantum well of 15 nm or greater should allow modulation at 1.55 μm at 300 K in a low voltage device. Of course operation of a device at higher temperatures will also result in longer wavelength operation due to the thermal shrinking of the bandgap[6, 13]. The wider quantum wells will also result in less spatial overlap of the wavefunctions and therefore there will be some maximum value of quantum well width above which the modulation with electric field will be too small to be useful due to the reduced absorption. Further modeling is required to determine this value and it is beyond the scope of the present paper.

VII. CONCLUSIONS

To conclude, an 8-band **k.p** tool has been used to model and simulate the absorption spectra of a number of Ge quantum well structures. To accurately agree with experimental devices grown on thin virtual substrates the substrates had to have tensile strain applied while for thick graded buffers, the experimental results agree with theory without any strain in the virtual substrate. The excellent agreement between theory and experiment demonstrates that the direct bandgap absorption dominates the device characteristics especially at low electric fields and low temperatures. The tool was also used to predict the performance of z-polarized waveguide geometry devices along with mapping out the useful energy space over which such modulators could be applied.

Acknowledgments

The author would like to acknowledge the support of Stefan Birner with the Nextnano software along with useful discussions with Paul Stavrinou and Jing Zhang.

[1] R. A. Soref and B. R. Bennett, IEEE J. Quant. Electron. **QE23**, 123 (1987).
[2] R. A. Soref, Proc. IEEE **81**, 1687 (1993).
[3] A. Liu, R. Jones, L. Liao, D. Samara-Rubio, D. Rubin, O. Cohen, R. Nicolaescu, and M. Paniccia, Nature (London) **427**, 615 (2004).
[4] Q. Xu, B. Schmidt, S. Pradhan, and M. Lipson, Nature (London) **435**, 325 (2005).
[5] Y. H. Kuo, Y. K. Lee, Y. Ge, S. Ren, T. Kamins, D. A. B. Miller, and J. S. Harris, Nature (London) **437**, 1334 (2005).
[6] Y. H. Kuo, Y. K. Lee, Y. Ge, S. Ren, J. E. Roth, T. I. Kamins, D. A. B. Miller, and J. S. Harris, IEEE J. Select Topics Quant. Elec. **12**, 1503 (2006).
[7] D. A. B. Miller, D. S. Chemla, T. C. Damen, A. C. Gossard, W. Wiegmann, T. H. Wood, and C. A. Burrus, Phys. Rev. Lett. **53**, 2173 (1984).
[8] D. A. B. Miller, D. S. Chemla, T. C. Damen, A. C. Gossard, W. Wiegmann, T. H. Wood, and C. A. Burrus, Phys. Rev. B **32**, 1043 (1985).
[9] S. Tsujino, H. Sigg, G. Mussler, D. Chrastina, and H. von Känel, Appl. Phys. Lett. **89**, 262119 (2006).
[10] URL `http://www.wsi.tu-muenchen.de/nextnano3/`.
[11] G. Bastard, *Wave Mechanics Applied to Semiconductor Heterostructures* (Monograph de Physique, Paris, 1988).
[12] Landolt-Börnstein, ed., *Band 17 Halbleiter* (Springer-Verlag, Berlin, 1982).
[13] Y. P. Varshni, Physica **34**, 149 (1968).
[14] C. G. V. de Walle, Phys. Rev. B **39**, 1871 (1989).
[15] L. D. Laude, F. H. Pollak, and M. Cardona, Phys. Rev. B **3**, 2623 (1971).
[16] M. Chandrasekhar and F. H. Pollak, Phys. Rev. B **15**, 2127 (1977).
[17] S.-H. Wei and A. Zunger, Phys. Rev. B **60**, 5404 (1999).
[18] C. G. van de Walle and R. M. Martin, Phys. Rev. B **34**, 5621 (1986).
[19] G. S. Cargill, J. Angilello, and K. L. Kavanagh, Phys. Rev. Lett. **61**, 1748 (1988).
[20] I. Balslev, Phys. Rev. **143**, 636 (1966).
[21] M. M. Rieger and P. Vogl, Phys. Rev. B **48**, 14276 (1993).
[22] D. J. Paul, Semicond. Sci. Technol. **19**, R75 (2004).
[23] I. Vurgaftman, J. R. Meyer, and L. R. Ram-Mohan, J. Appl. Phys. **89**, 5815 (2001).
[24] R. W. Kelsall, Z. Ikonic, C. R. Pidgeon, P. J. Philips, P. Harrison, S. A. Lynch, P. Townsend, D. J. Paul, S. L. Liew, D. J. Norris, et al., Phys. Rev. B **71**, 115326 (2005).
[25] S. A. Lynch, D. J. Paul, P. Townsend, G. Matmon, Z. Suet, R. Kelsall, Z. Ikonic, P. Harrison, J. Zhang, D. Norris, et al., IEEE J. Selected Topics Quant. Electron. **12**, 1570 (2006).
[26] M. Califano, N. Q.Vinh, P. J. Phillips, Z. Ikonic, R. W. Kelsall, P. Harrison, C. R. Pidgeon, B. N. Murdin, D. J. Paul, P. Townsend, et al., Phys. Rev. B **75**, 045338 (2007).
[27] T. Fromherz, M. Meduna, G. Bauer, A. Borak, C. V. Falub, S. Tsujino, H. Sigg, and D. Grützmacher, J. Appl. Phys. **98**, 044501 (2005).
[28] J. Liu, D. D. Cannon, K. Wada, Y. Ishikawa, D. T. Danielson, S. Jongthammanurak, J. Michel, and L. C. Kimerling, Phys. Rev. B **70**, 155309 (2004).
[29] J. Liu, D. Cannon, K. Wada, Y. Ishikawa, S. Jongthammanurak, D. T. Danielson, J. Michel, and L. C. Kimerling, Appl. Phys. Lett. **87**, 011110 (2005).